HHS Public Access

Author manuscript

Dev Cell. Author manuscript; available in PMC 2017 April 18.

Published in final edited form as:

Dev Cell. 2016 April 18; 37(2): 174–189. doi:10.1016/j.devcel.2016.03.023.

Polo Kinase Phosphorylates Miro to Control ER-Mitochondria Contact Sites and Mitochondrial Ca^{2+} Homeostasis in Neural Stem Cell Development

Seongsoo Lee[#1,2,#], **Kyu-Sun Lee**[#1,2], **Sungun Huh**[#1], **Song Liu**[1], **Do-Yeon Lee**[1], **Seung Hyun Hong**[2], **Kweon Yu**[2], and **Bingwei Lu**[1,*]

[1] Department of Pathology, Stanford University School of Medicine, Stanford, CA 94305, USA

[2] BioNanotechnology Research Center, Korea Research Institute of Biotechnology and Bioscience, Daejeon, 305-806, Korea

[#] These authors contributed equally to this work.

SUMMARY

Mitochondria play central roles in buffering intracellular Ca^{2+} transients. While basal mitochondrial Ca^{2+} (Ca^{2+}_{mito}) is needed to maintain organellar physiology, Ca^{2+}_{mito} overload can lead to cell death. How Ca^{2+}_{mito} homeostasis is regulated is not well understood. Here we show that Miro, a known component of the mitochondrial transport machinery, regulates *Drosophila* neural stem cell (NSC) development through Ca^{2+}_{mito} homeostasis control independent of its role in mitochondrial transport. Miro interacts with Ca^{2+} transporters at the ER-mitochondria contact site (ERMCS). Its inactivation causes Ca^{2+}_{mito} depletion and metabolic impairment, whereas its overexpression results in Ca^{2+}_{mito} overload, mitochondrial morphology change, and apoptotic response. Both conditions impaired NSC lineage progression. Ca^{2+}_{mito} homeostasis is influenced by Polo-mediated phosphorylation of a conserved residue in Miro, which positively regulates Miro localization to, and the integrity of, ERMCS. Our results elucidate a regulatory mechanism underlying Ca^{2+}_{mito} homeostasis and how its dysregulation may impact NSC metabolism/development and contribute to disease.

Graphical Abstract

[*] To whom correspondence should be addressed: bingwei@stanford.edu.
[#]Current Address: Gwangju Center, Korea Basic Science Institute, Gwangju, 500-757, Korea

Author Contributions

S.Lee, K-S.L and S.H. designed the study, performed the experiments, analyzed data, wrote the manuscript, and contributed equally. S.Liu., D-Y.L, and S.H.H performed some of the experiments and contributed data. K.Y. participated in the supervision of the study and provided key reagents. B.L. conceived and supervised the study and wrote the manuscript.

See Extended Experimental Procedures for additional details.

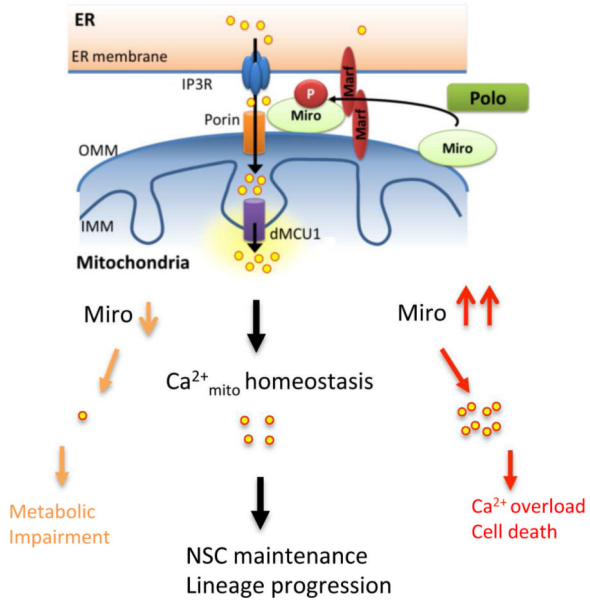

INTRODUCTION

Mitochondria are important for many aspects of cellular function, from ATP production and intermediary metabolism to apoptosis. Mitochondrial dysfunction has been broadly linked to the pathogenesis of a multitude of neurological disorders (Chan, 2006; Schon and Przedborski, 2011; Tait and Green, 2012; Wallace, 2005), emphasizing the particular importance of this organelle to neuronal function and maintenance. Mitochondrial function and Ca^{2+} signaling have been intimately linked. On one hand, Ca^{2+}_{mito} uptake helps buffer cytosolic Ca^{2+} signals and oscillations such as those generated by neuronal activation, thus amplifying and sustaining signals arising from neuronal activity while protecting neurons from the potentially damaging Ca^{2+} spikes (MacAskill et al., 2010; Sheng and Cai, 2012; Vos et al., 2010). On the other hand, Ca^{2+}_{mito} can positively regulate the activities of TCA cycle enzymes and electron transport chain components, stimulating ATP production (Cardenas et al., 2010; Jouaville et al., 1999; McCormack et al., 1990). Ca^{2+}_{mito} uptake primarily occurs at ERMCS where local Ca^{2+} can reach high levels (Rizzuto et al., 1993; Rizzuto et al., 1998). Proteins localized to ERMCS include those that mediate Ca^{2+} transfer, such as inositol 1,4,5-trisphosphate receptor (IP3R) at the ER, voltage-dependent anion-selective channel (VDAC) at the mitochondria outer membrane (MOM), mitochondrial Ca^{2+} uniporter (MCU) at the mitochondrial inner membrane (MIM) (Giorgi et al., 2015; Hajnoczky et al., 2002; Rowland and Voeltz, 2012), and mitofusin-2 (de Brito and Scorrano, 2008). In addition to transferring Ca^{2+}, ERMCS also transfer lipids (Hayashi et al., 2009). Despite the importance of ERMCS to fundamental cellular functions and its potential link to disease conditions (Schon and Area-Gomez, 2013; Rizzuto et al., 2012), its roles during normal development remain mostly unexplored, and the signaling mechanisms regulating its integrity and function are largely unknown.

Mitochondrial rho GTPase (Miro) is a MOM protein containing two GTPase domains and two Ca^{2+}-sensing EF hand domains (Fransson et al., 2003). Genetic studies in *Drosophila*

(Guo et al., 2005) and mouse (Nguyen et al., 2014) revealed a key function of Miro in regulating the axonal transport of mitochondria, during which Miro forms a multi-protein complex with Milton and Kinesin heavy chain (KHC) to link mitochondria with motor molecules and the microtubule cytoskeleton (Glater et al., 2006). Through binding to the EF hands of Miro and altering protein-protein interactions within the transport machinery, cytosolic Ca^{2+} dynamically regulates the motility of mitochondria, offering one mechanism to match mitochondrial distribution with neuronal activity (Macaskill et al., 2009; Saotome et al., 2008; Wang and Schwarz, 2009). The PINK1/Parkin pathway, which is critically involved in maintaining mitochondrial function and mutations in which are associated with Parkinson's disease (PD), can regulate Miro stability and thus mitochondrial transport (Liu et al., 2012; Wang et al., 2011). Interestingly, despite the importance of the Miro/Milton/Khc complex in regulating mitochondrial transport in metazoans, Miro is the only component conserved in all eukaryotes, suggesting that it may perform some ancestral function that is independent of the transport complex. Indeed, functions of Miro not directly related to transport are emerging in yeast (Lee and Lu, 2014), where yeast Miro (Gem1) is localized to ERMCS (Kornmann et al., 2011) and regulates ER-associated mitochondrial division (Murley et al., 2013). The prominent roles of Miro in mitochondrial regulation and the importance of mitochondria to neuronal function and survival in humans promoted us to examine the physiological role of Miro in the nervous system of a multicellular organism.

RESULTS

Miro Regulates *Drosophila* NSC Maintenance in a Manner Independent of Mitochondrial Transport

To investigate the physiological function of Miro in a developmental setting, we used *Drosophila* central brain NSCs called NBs. We examined the type I and type II NBs in the larval brains of animals carrying the $dMiro^{B682}$ mutant allele, presumably a protein null (Figure S1A, S1B) with disrupted mitochondrial distribution in neuronal and muscle tissues and late-larvae or early-pupae lethality (Guo et al., 2005). The brain size and number of Deadpan (Dpn)-positive NBs were dramatically reduced in $dMiro^{B682}$ homozygous mutants (Figure 1A, 1B). Loss of NB was also observed when dMiro was specifically knocked down in the NB lineages by RNAi (Figure 1C, 1D). To examine the effect of *dMiro* mutation on NB lineage architecture, we performed clonal analysis with MARCM (Lee and Luo, 2001). Type I and type II NB lineages of control animals each invariably contained one Dpn-positive primary NB, whereas the primary NBs were frequently lost in $dMiro^{B682}$ mutant NB clones (Figure 1E). In cases where the primary NBs remained in the mutant clones, their sizes were noticeably smaller than control NBs (Figure 1E, 1F). These results indicate a critical and cell-autonomous role of Miro in the development and/or maintenance of larval brain NBs.

Type II NBs undergo self-renewing asymmetric divisions to generate immature intermediate progenitors (IPs), which progress into transit-amplifying mature IPs that also undergo self-renewing asymmetric divisions to generate ganglion mother cells (GMCs) and differentiated neuronal or glial progenies (Bello et al., 2006; Boone and Doe, 2008; Bowman et al., 2008). IPs sequentially express the transcription factors Dichaete (D), Grainy head (Grh), and

Eyeless (Ey) during their transition from young to old IPs (Bayraktar and Doe, 2013). Thus, early-born (old) IPs express Ey, whereas late-born (young) IPs express D. In *dMiro*^{B682} mutant clones, young IPs and old IPs were both significantly reduced in number compared to control WT clones (Figure S1C, S1D). Loss-of-function (LOF) of dMiro thus reduces the number of transit-amplifying IPs, presumably as a result of stem cell loss during lineage progression.

Next, we examined Miro gain-of-function (GOF) effect using *1407-Gal4-* or *Pnt-Gal4-* directed pan-NB or type II NB-specific Miro overexpression (OE), respectively. Miro OE led to a reduction of the number of total NBs in *1407-Gal4>dMiro-OE* (Figure 1G, 1I) and occasional loss of type II NBs in *Pnt-Gal4>dMiro-OE* conditions (Figure 1H, 1J). A reduction of NB size was also seen in dMiro-OE animals (Figure 1K, 1L). In the *Pnt-Gal4>dMiro-OE* condition, the number of IPs, specifically the D^+ young IPs in type II NB lineages, was reduced (Figure 1M). These results indicate that NB maintenance and lineage progression are sensitive to Miro dosage.

Miro is a key component of a conserved protein complex that transports mitochondria along microtubule tracks (Brickley et al., 2005; Fransson et al., 2006; Guo et al., 2005; Hirokawa, 1998; Pilling et al., 2006; Stowers et al., 2002). To test whether the function of Miro in mitochondrial trafficking is important for NB maintenance, we examined mitochondrial distribution in *dMiro* mutant clones by staining for ATPsyn5α. Mitochondrial distribution or morphology was not obviously affected by *dMiro* mutation in NB lineages (Figure S1E). To further assess the role of mitochondrial transport in NB development, we analyzed the LOF and GOF of Milton, another key component of the transport complex (Glater et al., 2006). Neither the number nor size of primary NBs was affected by NB-specific knockdown of Milton (Figure S1F), in *milton*^{92} mutant MARCM clones (Figure 1E, 1F), or when Milton was overexpressed (Figure 1I, 1J). The *Milton RNAi* line used here was known to be effective in altering neuronal mitochondrial transport or function (Liu et al., 2012; Fang et al., 2012; Iijima-Ando et al., 2009). Intriguingly, Miro-OE led to mitochondrial distribution defects in NBs, with mitochondria accumulating asymmetrically to one side of the perinuclear area, and this defect was partially rescued by Milton-RNAi (Figure S1G). However, Miro-OE effect on NB lineage development was not affected by Milton-RNAi (data not shown), suggesting that a transport-independent function of Miro is important for NB maintenance and lineage development.

Miro Regulates Ca^{2+}_{mito} Homeostasis

Miro contains GTPase domains and Ca^{2+}-binding EF hand motifs, and its function in transporting neuronal mitochondria is regulated by activity-induced Ca^{2+} influx (Macaskill et al., 2009; Saotome et al., 2008; Wang and Schwarz, 2009). Yeast Gem1 and mammalian Miro1 (Rhot1) are localized to ERMCS (Kornmann et al., 2011), a structure that directs Ca^{2+} transfer from ER to mitochondria (Hayashi et al., 2009). To test whether Miro regulates Ca^{2+}_{mito} homeostasis in NSC lineage, we first measured Ca^{2+}_{mito} levels under dMiro LOF and GOF, using the Ca^{2+}-sensitive fluorescent dye Rhod-2 AM. Consistent with a previous study (Guo et al., 2005), Rhod-2 AM preferentially monitored Ca^{2+}_{mito} in *Drosophila* neurons (Figure S2A). We loaded primary cultured neurons with Rhod-2 AM.

Blocking ER Ca^{2+} uptake with thapsigagin (TG) increased cytosolic Ca^{2+} and induced a spike of Ca^{2+}_{mito} as reported (Perocchi et al., 2010), which quickly dissipated in control cells. Notably, in Miro-OE neurons the TG-induced Rhod-2 AM spike was stronger and persisted longer (Figure 2A), whereas TG induced a much weaker spike in *dMiro*^{B682} mutant or Miro-RNAi neurons than controls (Figure 2B, 2C). We also measured cytosolic Ca^{2+} response using Fluo-3AM. Overexpression of wild type but not a mutant form of Miro led to a decrease in the magnitude of cytosolic Ca^{2+} spikes induced by TG (Figure S2B).

To detect Ca^{2+}_{mito} levels *in vivo* in NBs, we expressed genetically-encoded, mitochondria-targeted Ca^{2+}_{mito} reporters mito-Apoeaquorin (mtAEQ) (Terhzaz et al., 2006) or mito-GCaMP3 (Lutas et al., 2012) in type II NBs. With the mtAEQ reporter, dissected brains from transgenic (Tg) animals were treated with histamine, an IP3-generating agonist, to induce Ca^{2+} release from the ER and increase Ca^{2+}_{mito} uptake (Perocchi et al., 2010), and luminescence signals were immediately measured with an automated luminometer. Under this condition, Ca^{2+}_{mito} was significantly elevated when known components of ERMCS such as Marf and Porin/VDAC were overexpressed, and Ca^{2+}_{mito} was attenuated when they were inhibited (Figure 2E, 2F), validating the utility of the reporters in monitoring the effect of ERMCS on Ca^{2+}_{mito} homeostasis. We found that Ca^{2+}_{mito} was significantly increased by Miro-OE, but decreased by Miro-RNAi (Figure 2D). In contrast, Milton LOF or GOF had no obvious effect on Ca^{2+}_{mito} uptake under similar conditions (Figure S2C). With the mito-GCaMP3 reporter, we observed that basal fluorescence signal was significantly increased by Miro-OE or Porin-OE (Figure 2G, 2H). The expression level of mito-GCaMP protein was not altered by Miro-OE (Figure S2D). These results, and the observation that cytosolic Ca^{2+} level as measured with a cytosolic GCaMP reporter (Figure S2E-F), and mitochondrial membrane potential (Figure S2G, S2H) - the driving force of Ca^{2+}_{mito} entry, were not altered by Miro-OE, support that Miro specifically promotes Ca^{2+}_{mito} uptake. Miro therefore regulates Ca^{2+} transfer from ER to mitochondria, and this occurs in a manner seemingly independent of mitochondrial transport.

Miro-Mediated Ca^{2+}_{mito} Homeostasis Regulates Mitochondrial Activity

Ca^{2+}_{mito} uptake critically regulates many cellular functions, ranging from ATP production to cell death (Rizzuto et al., 2012). Sufficient Ca^{2+} uptake into the mitochondrial matrix is needed for ATP production by enhancing the activities of key metabolic enzymes. For example, the key TCA cycle enzyme pyruvate dehydrogenase (PDH) is inhibited by phosphorylation by PDH kinase (PDK). Ca^{2+}_{mito} activates PDH phosphatase to remove an inhibitory phosphate from PDHE1 subunit (Cardenas et al., 2010). Thus, Ca^{2+}_{mito} negatively influences p-PDHE1 level. Normalized p-S293-PDHE1 level was markedly increased in *dMiro* mutant but decreased in Miro-OE brain extracts (Figure 3A, 3B, S3A, S3B). Consistently, the intensity of p-PDHE1 immunosignal was increased in *dMiro* mutant but decreased in Miro-OE NB clones, compared to control NBs located outside of the clones in the same animals (Figure 3C). ATP production in larval brain was decreased in *dMiro*^{B682} mutant, which was rescued by NB-specific Miro-OE (Figure 3G). Measurement of oxygen consumption rate (OCR) confirmed alteration of mitochondrial metabolism under Miro LOF and GOF conditions (Figure 3H). In response to ATP depletion, AMP-activated protein kinase (AMPK) is activated by phosphorylation as a compensatory response to restore

energy homeostasis (Hardie, 2007). AMPK was hyperphosphorylated in *dMiro* mutant (Figure 3A, 3B). These results suggest that reduced Ca^{2+}_{mito} uptake impairs mitochondrial metabolism and ATP production in Miro LOF condition.

While mitochondrial metabolism requires sufficient levels of Ca^{2+}_{mito}, prolonged Ca^{2+}_{mito} uptake can lead to opening of the permeability transition pore and release of pro-apoptotic components such as Cytochrome (Cyt) *c*, a critical event in mitochondria-mediated cell death (Rizzuto et al., 2012). To test whether the detrimental effect of Miro-OE on NB maintenance is related to Ca^{2+}_{mito} overload-induced cytotoxicity, we analyzed mitochondrial redox status using MitoSOX Red, a mitochondrial superoxide indicator. MitoSOX signal was higher in Miro-OE than control clones. No obvious change in MitoSOX signal was observed in *dMiro* mutant clones (Figure 3D, 3E). Miro-OE but not *dMiro* mutant clones also showed increased staining of activated caspase-3 (Figure 3F), and release of Cyt *c* into the cytosol (Figure S3C, S3D), which are markers of apoptotic processes.

Under normal physiological conditions, the bulk of cellular Ca^{2+} resides within the ER lumen. ER Ca^{2+} depletion can cause ER stress and activate an unfolded protein response (Malhotra and Kaufman, 2011). We tested whether, by enhancing Ca^{2+}_{mito} uptake, Miro-OE might lower ER luminal Ca^{2+} level and cause ER stress. The ER stress marker p-eIF2α was significantly elevated in Miro-OE but not *dMiro* mutant NB clones (Figure S3E), suggesting that elevated Ca^{2+}_{mito} uptake may cause Ca^{2+}_{mito} overload, Ca^{2+} depletion from the ER, and ER stress, all of which may contribute to apoptotic responses in Miro-OE condition. To test this hypothesis, we first examined the effect of ER stress inducers on NB development. Acute treatment of 3rd instar larvae with 5mM DTT + 1μM TG resulted in loss of IPs (Figure S3G), indicating that ER stress can recapitulate Miro-OE effect in NB development. Importantly, two independent RNAi lines against the ER stress kinase PERK both effectively rescued dMiro-OE induced NB lineage defects (Figure S3F). Next, we estimated ER Ca^{2+} content by measuring ionomycin-releasable Ca^{2+} levels (Tu et al., 2006). Ionomycin is an ionophore that causes more complete emptying of ER Ca^{2+} stores than TG. In the absence of extracellular Ca^{2+}, ionomycin elevates intracellular (cytosolic) Ca^{2+} by emptying intracellular stores, and the resulting transient Ca^{2+} peak gives a reasonable approximation of steady state ER Ca^{2+} content. With this method, we found that HeLa cells transfected with hMiro1 have less ER Ca^{2+} content than control cell transfected with empty vector (Figure S3H, I). Together, these results indicate that Miro-regulated Ca^{2+} homeostasis within the ER and mitochondria are both important for NB lineage development.

Miro Interacts with Ca^{2+} Transporters at the ERMCS to Regulate Ca^{2+}_{mito} Homeostasis and NB Maintenance

Transfer of Ca^{2+} from the ER to mitochondria is a major function of the ERMCS carried out by the Ca^{2+} transporters IP3R, VDAC, and MCU localized at the ER, MOM, and MIM respectively. We found that similar to Miro case, knocking down fly IP3R (Venkatesh and Hasan, 1997), Porin (VDAC) (Messina et al., 1996), or MCU resulted in reduced NB number (Figures S4A-S4D), supporting the importance of ER-mitochondria Ca^{2+} transfer to NB maintenance. In addition, overexpressing these Ca^{2+} transporters also modestly reduced NB number (Figure S4E, S4F). We further tested the genetic interaction between Miro and

the Ca^{2+} transporters. Although the heterozygous conditions for *dMiro* or each of the Ca^{2+} transporter genes alone had no obvious effect on NB development, double heterozygous combinations between *dMiro* and the Ca^{2+} transporters resulted in reduced NB number (Figure 4A, 4B), supporting that Miro functionally interacts with Ca^{2+} transporters at the ERMCS to control Ca^{2+}_{mito} homeostasis, mitochondrial function, and NB maintenance. Consistently, partial LOF of IP3R or Porin reduced Ca^{2+}_{mito} to basal levels in Miro-OE condition and blocked the Miro-OE effect on NB maintenance (Figure S4G, S4H).

We next took a pharmacological approach to test the role of Ca^{2+}_{mito} homeostasis in mediating Miro function in NSCs. Previous studies showed that feeding flies with $CaCl_2$ could increase intracellular Ca^{2+} levels, especially at the larval stage (Dube et al., 2000), and that exogenous Ca^{2+} could overcome genetic deficits in intracellular Ca^{2+} signaling (Howard, 1984). We found that Ca^{2+}_{mito} was increased upon $CaCl_2$ feeding (Figure S4I, S4J), and that feeding $dMiro^{B682}$ mutant larvae with $CaCl_2$ partially restored ATP production (Figure 4C) and rescued the brain size reduction and NB loss (Figure 4D). Conversely, Ca^{2+}_{mito} overload caused by Miro-OE was attenuated (Figure S4I, S4J), and the reduction of NB size and loss of IPs in *Pnt>Miro-OE* condition was rescued by reducing Ca^{2+}_{mito} level via Ca^{2+} chleation with bis (2-aminophenoxy) ethane tetra-acetic acid (BAPTA), or IP3R inhibition with 2-aminoethoxydiphenyl borate (2-APB) (Figure 4E, 4F).

We also tested the interaction between Miro and the ER-mitochondria Ca^{2+} transporters using available GOF alleles. NB-specific OE of Porin or dMCU significantly rescued the NB-loss phenotype seen in $dMiro^{B682}$ mutant (Figure 4G, 4H). Consistent with mitochondrial metabolic impairment due to reduced Ca^{2+}_{mito} uptake being responsible for the NB phenotype in $dMiro^{B682}$ mutant, overexpression of yeast NDI1 (yNDI1), which encodes a single-peptide alternative complex-I and is functional in boosting fly mitochondrial complex-I activity (Bahadorani et al., 2010; Sanz et al., 2010), partially restored NB number in $dMiro^{B682}$ mutant. Enhancing PDH activity by PDK RNAi had similar effect (Figure 4G, 4H). This contrasts with the lack of effect of overexpressing the apoptosis inhibitor p35 (data not shown), or the compound removal of three cell death executers in flies (Reaper, Grim, and Hid) using the *H99* deficiency (Foley and Cooley, 1998) (Figures 4G, 4H). These results support the notion that the Miro-LOF effect on NB maintenance is due to Ca^{2+}_{mito} depletion and metabolic impairment as apposed to Ca^{2+}_{mito} overload and apoptotic activation in Miro-GOF condition.

Regulation of Miro Function by Polo-Mediated Phosphorylation at Serine 66

Despite the importance of ER-mitochondria Ca^{2+} signaling to cellular physiology, little is known how this process is regulated. Implication of Miro as a key player in this process offers the opportunity to investigate the regulatory mechanisms. By aligning the sequence of Miro homologs from fly to humans, we identified a conserved, putative phosphorylation site for Polo-like kinases (PLKs) in the N-terminal GTPase domain of Miro (Figure 5A, S5A). Of the two GTPase domains of Miro, the N-terminal one is particularly important for ERMCS localization (Kornmann et al., 2011), mitochondrial morphology and transport, and cell survival (Babic et al., 2015). Polo is also of particular interest as previous studies identified it as a regulator of NB self-renewal in *Drosophila* (Wang et al., 2007). Our

immunohistochemical and biochemical analyses indicated that a fraction of Polo protein is localized to mitochondria (Figure S5B-E). To test for a molecular link between Miro and Polo in NB maintenance, we first asked whether Miro and Polo physically interact *in vivo*. In co-IP experiments using *elav>Polo-GFP* fly head extracts, we detected Polo-GFP in complex with endogenous dMiro (Figure 5B). Co-expression with Polo resulted in increased dMiro phosphorylation at Ser but not Thr residue(s) (Figure 5C, 5D). To test whether Polo directly phosphorylates Miro, we performed *in vitro* kinase assays using PLK1 as kinase and GST-dMiro fusion proteins as substrates. PLK1 strongly phosphorylated Miro-FL (aa 1-634) and Miro-N (aa 1–213), but not Miro-M (aa 210-393) or Miro-C (aa 390-634) (Figure 5E). None of the GST-Miro fusion proteins was phosphorylated by a control kinase PKC-zeta (Figure S5F, G). We next searched for the target site of Polo in Miro-N by focusing on conserved Ser residues, including Ser66 that matches the consensus site for PLKs (Figure 5A, S5A). We note that the corresponding sites in mammalian Miro1 and Miro2 may be better targets for PLK2 or 3, which prefers an acidic residue at +1 position (Rozeboom and Pak, 2012). A S66A mutation led to a dramatic reduction of Miro-N phosphorylation by PLK1 compared to mutating other conserved Ser residues (Figure 5F). S66 in dMiro N-terminal GTPase domain thus represents a major phosphorylation site for PLK1 *in vitro*.

To study the physiological effects of Polo-mediated phosphorylation of Miro *in vivo*, we generated Tgs expressing wild type dMiro (dMiro-WT) or dMiro-S66A. To circumvent overexpression artifacts, Tgs that express dMiro-WT and dMiro-S66A at comparable, but less than endogenous dMiro expression levels (Figure 6F, S3A), were chosen for further analyses. The NB-loss phenotype seen in *dMiro* mutant was significantly rescued by *1407-Gal4*-driven expression of dMiro-WT but not dMiro-S66A (Figure 5G, 5H). This effect is likely related to the function of Miro in modulating Ca^{2+}_{mito} homeostasis, as dMiro-S66A exhibited compromised ability to induce Ca^{2+}_{mito} uptake compared to dMiro-WT (Figure S5H, S2B). Similarly, reduced ATP production in *dMiro* mutant larval brain was rescued by *1407-Gal4* driven dMiro-WT, but not -S66A (Figure 5I). Unlike in dMiro-WT case, NB clones overexpressing dMiro-S66A did not show increased mitochondrial ROS (Figure S5J). Phosphorylation of S66 in dMiro thus positively influences its function in regulating mitochondrial function and NB maintenance under basal conditions.

Consistent with Polo playing a role in regulating Ca^{2+}_{mito} homeostasis, Ca^{2+}_{mito} level was increased by Polo-OE but moderately decreased by Polo-RNAi (Figure S5I). Moreover, Polo-OE caused significant loss of type II NBs and IPs, which was rescued by dMiro RNAi or dMiro-S66A co-expression (Figure 5J-L), or by RNAi of genes mediating ER-mitochondria Ca^{2+} transfer (Figure 5M, 5N). Importantly, the NB and IP loss caused by Polo-OE was also partially rescued by pharmacological interventions that reduce Ca^{2+}_{mito} (Figure S5K, L). This effect was specific, as NB and IP losses caused by Numb-OE (Ouyang et al., 2011) was not rescued by similar treatments (Figure S5M). The Polo-Miro axis thus plays a physiological role in regulating NB maintenance via Ca^{2+}_{mito} homeostasis.

Phosphorylation of Miro by Polo Regulates the Integrity of ERMCS

We next sought to understand the mechanism by which Polo phosphorylation of Miro affects Ca^{2+}_{mito} homeostasis. We first tested whether phosphorylation affects the localization of

Miro. For this purpose, we generated an antibody against dMiro phosphorylated at S66 (p-S66-Miro), the specificity of which was demonstrated by the absence of signal in *dMiro* mutant (Figure S6A-C), its sensitivity to phosphatase treatment (Figure S6D), and its response to altered Polo activity (see later). To specifically examine the localization of Miro or p-S66-Miro with respect to mitochondria and ER, we used red fluorescent protein (RFP) tagged with the ER-retention sequence KDEL, or ER resident protein PDI tagged with GFP as ER markers, and ATPsyn5α as mitochondrial marker. Compared to the rather uniform mitochondrial localization of Miro protein in general, p-S66-Miro exhibited a granular localization pattern that colocalized with ATPsyn5α and overlapped extensively with ER markers in the perinuclear area (Figure 6A, B, D). The abundance of p-S66-Miro in the perinuclear area was reduced by Polo RNAi but increased by Polo-WT or constitutively active Polo (Polo-CA) OE (Figure 6C, E). Phosphorylation of Miro by Polo at S66 thus promotes its localization to the ERMCS.

To test whether Miro interacts with proteins localized to ERMCS and whether this interaction is affected by its phosphorylation status, we performed co-IP assays using fly brain tissues expressing dMiro-WT, dMiro-S66A, or phospho-mimetic dMiro-S66E, which functioned similarly as dMiro-WT in NBs when overexpressed (Figure 6F, 5I). Tg expression was driven by the pan-neuronal *elav-Gal4* driver. Miro-WT exhibited physical association with VDAC/Porin and Mitofusin/Marf, two key components of the ERMCS (de Brito and Scorrano, 2008; Rowland and Voeltz, 2012). Importantly, the Miro-Porin and Miro-Marf interactions were significantly enhanced by S66E, whereas the Miro-Marf interaction was attenuated by S66A mutation (Figure 6F, H), suggesting that S66 phosphorylation positively influences the interaction of Miro with proteins at the ERMCS.

We next examined the effect of Miro phosphorylation on ERMCS integrity. To this end, we analyzed the IP3R-VDAC interaction in brain tissues of *dMiro* mutant or Tg flies expressing Miro variants. Although the expression level of IP3R or VDAC was unaltered in all genotypes tested, their physical association was reduced in *dMiro* mutant or Miro-S66A Tg tissues, but increased in Miro-WT or Miro-S66E Tg tissues (Figure 6G, I). Since S66 is located within the first GTPase domain of Miro, we examined the effect of S66 phosphorylation status on GTPase activity. *In vitro* GTPase assays showed time-dependent GTP hydrolysis by the N-terminal GTPase domain of Miro-WT and Miro-S66D or Miro-S66E, with phosphomimetic Miro exhibiting greater GTPase activity than Miro-WT (Figure S6E). Moreover, prior phosphorylation by Polo significantly enhanced the GTPase activity of Miro-WT, but not Miro-S66A (Figure S6F). We conclude that Polo-mediated phosphorylation positively regulates the GTPase activity of Miro and the recruitment of Miro to ERMCS, where p-S66-Miro enhances the integrity of this ER-mitochondria tethering complex.

Miro Plays Conserved Roles in Regulating Ca^{2+}_{mito} Homeostasis in Mammalian Cells

To test the conservation of the mechanisms of Miro function and regulation, we turned to the human cervical cancer cell line (HeLa) and mouse NSCs. Addition of IP3R agonist histamine to HeLa cells enhanced the recruitment of hMiro1 to the perinuclear ER area, and this effect was ameliorated by the co-treatment with BI2536, a specific chemical inhibitor of

PLK1 (Figure 7A, B, S7B). Monitoring Ca^{2+}_{mito} with Rhod-2 AM showed that Ca^{2+}_{mito} was significantly increased in cells transfected with dMiro-WT or -S66E, but less so with dMiro-S66A (Figure 7C, 7D). Previous studies showed that hMiro1 (Fransson et al., 2003) or dMiro (Liu et al., 2012) caused aberrant mitochondrial morphology when overexpressed. We found that hMiro1-induced mitochondrial aggregation in HeLa cells was attenuated by treatment with 2-APB or Ru360, cell-permeant pharmacological inhibitor of IP3R or MCU, respectively (Tang et al., 2005; Garcia-Rivas Gde et al., 2006), or by chelating Ca^{2+} with BAPTA-AM (Figure 7E), suggesting that Miro-regulated Ca^{2+}_{mito} homeostasis underlies its effect on mitochondrial morphology. Moreover, Myc-tagged dMiro-WT, -S66E, or -S66D exhibited more pronounced perinuclear and aggregated localization than Miro-S66A (Figure S7C). These results suggest that as in fly tissues, phosphorylation of Miro at S66 site promotes Miro localization to ERMCS in HeLa cells. We also examined the effect of Polo-Miro signaling on the integrity of the ER-mitochondria tethering complexes. The interaction between VDAC and IP3R was weakened by treatment with BI2536 (Figure 7F, 7G). Immunostaining with ER and mitochondrial markers reveal that ER-mitochondria interaction was increased in cell transfected with hMiro1-WT, but not with hMiro1-SA (Figure S7E, S7F), supporting a critical role of PLK signaling in ER-mitochondria interaction and Ca^{2+}_{mito} uptake. Finally, we examined the effect of Miro on the proliferation of mouse NSCs. Transfection of NSCs with hMiro1-WT attenuated NSC proliferation, whereas hMiro1-S59A (equivalent of dMiro-S66A) was less effective in this aspect (Figure 7H). Mitochondrial metabolism as monitored by OCR was increased by hMiro1-WT but decreased by hMiro1-SA in mouse NSCs (Figure S7G). Supporting the importance of ER-mitochondria Ca^{2+} transfer in NSC regulation, pharmacological inhibition of Ca^{2+}_{mito} uptake by Ru360, and to a lesser extent by 2-APB, attenuated NSC proliferation (Figure S7D).

DISCUSSION

Mitochondrial and Ca^{2+} signaling pathways are intimately connected in many aspects of cellular physiology, from metabolism and ATP production to cell death. Previous studies have emphasized the key role of Miro in regulating mitochondrial transport by sensing local elevation of cytosolic Ca^{2+} concentration elicited by neuronal activity. This mechanism links mitochondrial distribution to the subcellular need for Ca^{2+} buffering. In this study we demonstrate a conserved role of Miro in regulating Ca^{2+}_{mito} homeostasis in an apparently transport-independent manner. Miro localizes to ERMCS and interacts with its protein components. We further show that this function of Miro is regulated by Polo-mediated phosphorylation at a conserved site in the N-terminal GTPase domain. The identification of new regulators of Ca^{2+}_{mito} homeostasis offers the opportunity to elucidate how Ca^{2+}_{mito} uptake is controlled in different cell types of multicellular organisms, and how defects in this process may impact development and disease.

Our results identify the Polo/Miro signaling axis as an important regulator of Ca^{2+}_{mito} uptake. ER is a major source of Ca^{2+}_{mito}, which is transported to mitochondrial matrix through Ca^{2+} transporters located at the ERMCS. Despite detailed biophysical studies of Ca^{2+}_{mito} uptake, little is known how this process is regulated to meet the developmental and physiological needs of distinct cell types in a multicellular organism. We show that Miro is

localized to ERMCS, where it interacts with components of the ERMCS to modulate the integrity of this quasi-synaptic structure and the inter-organelle Ca^{2+} transfer. Our genetic and biochemical studies further identify Polo kinase as a key regulator of Miro-controlled Ca^{2+}_{mito} homeostasis. Polo-induced phosphorylation of Miro promotes the localization of Miro to ERMCS, enhancing the interaction between Miro and components of the ER-mitochondria tethering complex and the integrity of the tethering complex. Our identification of S66 in the N-terminal GTPase domain as a key regulatory site of Miro is consistent with the known importance of this GTPase domain to Miro function (Kornmann et al., 2011; Babic et al., 2015). Our results also uncover a new mechanism of action for Polo in NSC self-renewal and differentiation. Dysregulation of PLKs has been implicated in cancer (Craig et al., 2014) and neurodegenerative diseases such as PD (Mbefo et al., 2010). Given that Miro OE-induced cell death involves Ca^{2+}_{mito} overload, mitochondrial dysfunction, oxidative stress, ER stress, and caspase 3 activation, key features broadly implicated in neurodegenerative diseases, it would be interesting to test in various disease conditions whether disease-causing genes or signaling pathways converge on Miro, and whether pharmacological inhibition of PLK-Miro signaling may offer broad therapeutic benefits.

Our analyses of the effect of Miro LOF and GOF in the fly NB lineages reveal a critical role of Ca^{2+}_{mito} homeostasis in cell fate determination. Miro LOF and GOF both impairs NB maintenance and lineage development, but through different mechanisms. Miro LOF causes Ca^{2+}_{mito} depletion and reduced ATP production, impairing cell growth, a key requirement of NB maintenance (Song and Lu, 2011), and causing premature differentiation and loss of NB stemness through a non-apoptotic mechanism. In contrast, Miro GOF causes Ca^{2+}_{mito} overload, oxidative stress, and activation of the apoptotic cascade, leading to failed maintenance of NB and IPs. These results reveal hypersensitivity of NSC maintenance and lineage progression to Ca^{2+}_{mito} levels. A role for Ca^{2+} signaling in progenitor maintenance was previously shown in the fly hematopoietic system (Shim et al., 2013). However, distinct from the importance of Ca^{2+}_{mito} to NB maintenance reported here, the maintenance of hematopoietic progenitors involves cytosolic Ca^{2+}, which is mediated by CaMKII signaling and is sensitive to SERCA activity (Shim et al., 2013), whereas NSC maintenance by Miro-mediated Ca^{2+}_{mito} homeostasis is insensitive to SERCA manipulation (data not shown). Together with previous studies implicating mitochondrial regulators or structural proteins in stem cell differentiation (Kasahara et al., 2013; Mitra et al., 2012; Lee et al., 2013; Teixeira et al., 2015), our result broadens the impact of mitochondria on developmental processes. Given the emerging connection between mitochondrial metabolism and epigenetic modifications (Wallace, 2010; Castegna et al., 2015), we speculate that there exist a mechanistic link between Miro-controlled Ca^{2+}_{mito} homeostasis and epigenetic regulation in the nucleus. Future studies will establish, at the molecular level, how developmental pathways dictating stem cell self-renewal vs. differentiation decision are connected with signaling pathways regulating mitochondrial function.

EXPERIMENTAL PROCEDURES

Fly Genetics

Fly culture and crosses were performed according to standard procedures and raised at indicated temperatures. To generate *UAS-dMiro-S66A* and *UAS-dMiro-S66E* Tg flies, wild-type *dMiro* cDNA was modified using the QuikChange Multi kit (Stratagene) to introduce the S66A and S66E mutations. The insert of *UAS-dMiro-WT-Myc* was replaced with *dMiro-S66A* and *dMiro-S66E* cDNAs to generate *UAS-dMiro-S66A-Myc* and *UAS-dMiro-S66E-Myc*, respectively. The resulting *pUAST-Miro* constructs were injected into w^- embryos to obtain Tg lines according to established procedures (Bestgene, Inc.).

MARCM and Flip-Out Clonal Analysis

To generate NB MARCM clones and overexpression clones, larvae at 24h after-larvae-hatching (ALH) were heat-shocked at 37°C for 90 min and further aged for 72 hrs at 25°C before dissection. MARCM analyses were performed essentially as described (Song and Lu, 2011). For making overexpression clones, *w, hsFLP; Actin 5c>CD2>Gal4, UAS-GFP-NLS* was crossed with the indicated *UAS* lines and 24h ALH larvae were heat-shocked at 37°C for 90 min and further aged for 72 hrs at 25°C before dissection.

Pharmacological Treatment

2-APB (Sigma), Ru360 (Calbiochem), EDTA/EGTA (Sigma), $CaCl_2$ (Sigma), BAPTA (Life Technologies), Histamine (Sigma), Thapsigargin (Calbiochem), or BI2536 (Selleckchem) dissolved in 0.5% DMSO was mixed in instant *Drosophila* media or cell culture at the indicated final concentrations. 0.5% DMSO alone was used as vehicle control. For treatment of flies, embryos were collected on drug-containing food or control food for 6 hrs at 25°C and allowed to develop further to 120 hr ALH before larval brain dissection and immunostaining.

Immunohistochemistry

To generate the p-S66 Miro antibody, a synthetic peptide with the sequence SIVDFpSAVEQS was used to elicit immune response in rabbits. Purification of the phospho-specific antibody was performed by AbFrontier (Seoul, Korea). Purified p-S66 antibody was diluted at 1:200 for immunostaining. For larval brain immunostaining, larvae were dissected in Schneider's medium (Invitrogen) and fixed with 4% formaldehyde in PEM buffer (100 mM PIPES at pH 6.9, 1 mM EGTA, 1 mM $MgCl_2$) for 23 min at room temperature. For ER-mitochondria interaction analysis, confocal image stacks were automatically thresholded using ImageJ. Colocalization between organelles was quantified using the Manders' algorithm (Manders et al., 1993).

Co-Immunoprecipitation and Western Blot Analyses

Approximately 25 adult fly thoraces were collected and homogenized in HBS buffer (210 mM Mannitol, 70 mM Sucrose, 5 mM HEPES pH 7.4, 1 mM EGTA) containing protease inhibitor (Sigma). The lysate was centrifuged at 1,300g for 10 min, and the supernatant was collected and centrifuged again at 13,000g for 15 min. For co-IP, the cytosolic and the

mitochondrial fractions were incubated with anti-GFP or anti-Myc conjugated protein G-agarose beads (Upstate) at 4 °C for 2 hours. Beads were washed 3x with PBS for 5 min each. Proteins were eluted and analyzed by WB as described (Wu et al., 2013).

In Vitro Kinase and GTPase Assays

The conditions of the in *vitro* kinase assays were essentially as described (Lee et al., 2010). GST-Miro fusion protein production was done as described (Liu et al., 2012). Briefly, cDNAs encoding fragments of dMiro were cloned into a glutathione S-transferase (GST)-encoding vector, pGEX-6P-1 (GE Healthcare), and GST fusion production was carried out in *E. coli* strain *BL21(DE3)* cells according to Manufacturer's instructions. PLK1 and PKC-zeta were purchased from ProQinase. The GTPase assay for dMiro was performed according to a published procedure (Koshiba et al., 2011).

ATP Measurement

The level of ATP in *Drosophila* larval brain was measured essentially as previously described (Wu et al., 2013), using a luciferase-based bioluminescence assay kit (ATP Bioluminescence Assay Kit HS II, Roche Applied Science).

Calcium Imaging

For calcium imaging in primary neural cells, ~50 third instar Tg larval brains expressing *Mito-GFP*, *Mito-GFP+UAS-dMiro-WT*, *Mito-GFP+UAS-dMiro-S66A*, or *Mito-GFP +dMiro RNAi* driven by *elav-GAL4* were collected. Primary neural cells were prepared according to published procedures (Egger et al., 2013). To monitor mitochondrial or cytosolic Ca^{2+} levels, primary neural cells were loaded with 1 μM Rhod-2 AM or Fluo-3 AM (Molecular Probes), respectively, in physiological salt solution [pH7.4] (150 mM NaCl, 4 mM KCl, 1 mM $MgCl_2$, 5.6 mM glucose, 5 mM HEPES) for 30 min at 37 °C. Primary neural cells were treated with 1 μM Thapsigargin (Calbiochem) for intracellular Ca^{2+} perturbation. Calcium imaging was carried out using an inverted confocal microscope (LSM 510 META and LIVE 5, Carl Zeiss) with a 40× objective.

For measuring mitochondrial Ca^{2+} in mammalian cells, HeLa cells were transfected with control *pCDNA3.0* vector or *Myc-hMiro1*, *Myc-hMiro2*, *Myc-dMiro-WT*, *Myc-dMiro-S66E*, or *Myc-dMiro-S66A* plasmids cloned in *pCDNA3.0*. After transfection, HeLa cells were loaded with Rhod-2 AM (10 μM in DMEM media, Molecular Probe) for 30 min at room temperature. Cells were then washed with DMEM for 30 min. Single cell fluorescence was excited at 545 nm and images of the emitted fluorescence obtained on a Leica TCS SP5 AOBS confocal microscope were processed with LAS AF (Leica).

Statistical Analysis

Statistical significance of all data were evaluated by two-tailed paired or unpaired Student's *t*-tests. For studies employing multiple testing, we used a one-way ANOVA followed by Bonferroni post hoc test. All data were presented as mean±s.e.m.

Supplementary Material

Refer to Web version on PubMed Central for supplementary material.

ACKNOWLEDGEMENTS

We are grateful to Drs. K Zinsmaier, DM Glover, J Lipsick, WM Saxton, D Smith, JK Chung, I Bezprozvanny, F Kawasaki, A. Whitworth, YN Jan, L Luo, M Guo, D Walker, S Davies, G Hasan, J Nambu, and the VDRC and Bloomington Stock Center for fly stocks and reagents. We thank members of the Lu laboratory for discussions and help. Supported by the NIH (R01NS083417 and R01MH080378 to BL), NRF (2014M3A908034462 to KL and 2015R1D1A1A01059079 to SL) and the Brainpool program of KOFST (to SL).

REFERENCE

Babic M, Russo GJ, Wellington AJ, Sangston RM, Gonzalez M, Zinsmaier KE. Miro's N-Terminal GTPase Domain Is Required for Transport of Mitochondria into Axons and Dendrites. J Neurosci. 2015; 35:5754–5771. [PubMed: 25855186]

Bahadorani S, Cho J, Lo T, Contreras H, Lawal HO, Krantz DE, Bradley TJ, Walker DW. Neuronal expression of a single-subunit yeast NADH-ubiquinone oxidoreductase (Ndi1) extends Drosophila lifespan. Aging Cell. 2010; 9:191–202. [PubMed: 20089120]

Bayraktar OA, Doe CQ. Combinatorial temporal patterning in progenitors expands neural diversity. Nature. 2013; 498:449–455. [PubMed: 23783519]

Bello B, Reichert H, Hirth F. The brain tumor gene negatively regulates neural progenitor cell proliferation in the larval central brain of Drosophila. Development. 2006; 133:2639–2648. [PubMed: 16774999]

Boone JQ, Doe CQ. Identification of Drosophila type II neuroblast lineages containing transit amplifying ganglion mother cells. Dev Neurobiol. 2008; 68:1185–1195. [PubMed: 18548484]

Bowman SK, Rolland V, Betschinger J, Kinsey KA, Emery G, Knoblich JA. The tumor suppressors Brat and Numb regulate transit-amplifying neuroblast lineages in Drosophila. Dev Cell. 2008; 14:535–546. [PubMed: 18342578]

Brickley K, Smith MJ, Beck M, Stephenson FA. GRIF-1 and OIP106, members of a novel gene family of coiled-coil domain proteins: association in vivo and in vitro with kinesin. J Biol Chem. 2005; 280:14723–14732. [PubMed: 15644324]

Cardenas C, Miller RA, Smith I, Bui T, Molgo J, Muller M, Vais H, Cheung KH, Yang J, Parker I, et al. Essential regulation of cell bioenergetics by constitutive InsP3 receptor Ca2+ transfer to mitochondria. Cell. 2010; 142:270–283. [PubMed: 20655468]

Castegna A, Iacobazzi V, Infantino V. The mitochondrial side of epigenetics. Physiol Genomic. 2015; 47:299–307.

Chan DC. Mitochondria: dynamic organelles in disease, aging, and development. Cell. 2006; 125:1241–1252. [PubMed: 16814712]

Craig SN, Wyatt MD, McInnes C. Current assessment of polo-like kinases as anti-tumor drug targets. Expt Opin Drug Disc. 2014; 9:773–789.

de Brito OM, Scorrano L. Mitofusin 2 tethers endoplasmic reticulum to mitochondria. Nature. 2008; 456:605–610. [PubMed: 19052620]

Dube KA, McDonald DG, O'Donnell MJ. Calcium homeostasis in larval and adult Drosophila melanogaster. Arch Insect Biochem Physiol. 2000; 44:27–39. [PubMed: 10790183]

Egger B, van Giesen L, Moraru M, Sprecher SG. In vitro imaging of primary neural cell culture from Drosophila. Nat Protocol. 2013; 8:958–965.

Fang Y, Soares L, Teng X, Geary M, Bonini NM. A novel Drosophila model of nerve injury reveals an essential role of Nmnat in maintaining axonal integrity. Curr Biol. 2012; 22:590–595. [PubMed: 22425156]

Foley K, Cooley L. Apoptosis in late stage Drosophila nurse cells does not require genes within the H99 deficiency. Development. 1998; 125:1075–1082. [PubMed: 9463354]

Fransson A, Ruusala A, Aspenstrom P. Atypical Rho GTPases have roles in mitochondrial homeostasis and apoptosis. J Biol Chem. 2003; 278:6495–6502. [PubMed: 12482879]

Fransson S, Ruusala A, Aspenstrom P. The atypical Rho GTPases Miro-1 and Miro-2 have essential roles in mitochondrial trafficking. Biochemi Biophysi Res Commun. 2006; 344:500–510.

Garcia-Rivas Gde J, Carvajal K, Correa F, Zazueta C. Ru360, a specific mitochondrial calcium uptake inhibitor, improves cardiac post-ischaemic functional recovery in rats in vivo. Br J Pharmacol. 2006; 149:829–837. [PubMed: 17031386]

Giorgi C, Missiroli S, Patergnani S, Duszynski J, Wieckowski MR, Pinton P. Mitochondria-associated membranes: composition, molecular mechanisms, and physiopathological implications. Antioxid Redox Signal. 2015; 22:995–1019. [PubMed: 25557408]

Glater EE, Megeath LJ, Stowers RS, Schwarz TL. Axonal transport of mitochondria requires milton to recruit kinesin heavy chain and is light chain independent. J Cell Biol. 2006; 173:545–557. [PubMed: 16717129]

Guo X, Macleod GT, Wellington A, Hu F, Panchumarthi S, Schoenfield M, Marin L, Charlton MP, Atwood HL, Zinsmaier KE. The GTPase dMiro is required for axonal transport of mitochondria to Drosophila synapses. Neuron. 2005; 47:379–393. [PubMed: 16055062]

Hajnoczky G, Csordas G, Yi M. Old players in a new role: mitochondria-associated membranes, VDAC, and ryanodine receptors as contributors to calcium signal propagation from endoplasmic reticulum to the mitochondria. Cell Calcium. 2002; 32:363–377. [PubMed: 12543096]

Hardie DG. AMP-activated/SNF1 protein kinases: conserved guardians of cellular energy. Nat Rev Mol Cell Biol. 2007; 8:774–785. [PubMed: 17712357]

Hayashi T, Rizzuto R, Hajnoczky G, Su TP. MAM: more than just a housekeeper. Trend Cell Biol. 2009; 19:81–88.

Hirokawa N. Kinesin and dynein superfamily proteins and the mechanism of organelle transport. Science. 1998; 279:519–526. [PubMed: 9438838]

Howard J. Calcium enables photoreceptor pigment migration in a mutant fly. J Exp Biol. 1984; 113:471–475.

Iijima-Ando K, Hearn SA, Shenton C, Gatt A, Zhao L, Iijima K. Mitochondrial mislocalization underlies Abeta42-induced neuronal dysfunction in a Drosophila model of Alzheimer's disease. PloS one. 2009; 4:e8310. [PubMed: 20016833]

Jouaville LS, Pinton P, Bastianutto C, Rutter GA, Rizzuto R. Regulation of mitochondrial ATP synthesis by calcium: evidence for a long-term metabolic priming. Proc Natl Acad Sci USA. 1999; 96:13807–13812. [PubMed: 10570154]

Kasahara A, Cipolat S, Chen Y, Dorn GW 2nd, Scorrano L. Mitochondrial fusion directs cardiomyocyte differentiation via calcineurin and Notch signaling. Science. 2013; 342:734–737. [PubMed: 24091702]

Kornmann B, Osman C, Walter P. The conserved GTPase Gem1 regulates endoplasmic reticulum-mitochondria connections. Proc Natl Acad Sci USA. 2011; 108:14151–14156. [PubMed: 21825164]

Koshiba T, Holman HA, Kubara K, Yasukawa K, Kawabata S, Okamoto K, MacFarlane J, Shaw JM. Structure-function analysis of the yeast mitochondrial Rho GTPase, Gem1p: implications for mitochondrial inheritance. J Biol Chem. 2011; 286:354–362. [PubMed: 21036903]

Lee KS, Lu B. The myriad roles of Miro in the nervous system: axonal transport of mitochondria and beyond. Front Cell Neurosci. 2014; 8:330. [PubMed: 25389385]

Lee KS, Wu Z, Song Y, Mitra SS, Feroze AH, Cheshier SH, Lu B. Roles of PINK1, mTORC2, and mitochondria in preserving brain tumor-forming stem cells in a noncanonical Notch signaling pathway. Genes Dev. 2013; 27:2642–2647. [PubMed: 24352421]

Lee S, Liu HP, Lin WY, Guo H, Lu B. LRRK2 kinase regulates synaptic morphology through distinct substrates at the presynaptic and postsynaptic compartments of the Drosophila neuromuscular junction. J Neuro Sci. 2010; 30:16959–16969.

Lee T, Luo L. Mosaic analysis with a repressible cell marker (MARCM) for Drosophila neural development. Trends Neurosci. 2001; 24:251–254. [PubMed: 11311363]

Liu S, Sawada T, Lee S, Yu W, Silverio G, Alapatt P, Millan I, Shen A, Saxton W, Kanao T, et al. Parkinson's Disease-Associated Kinase PINK1 Regulates Miro Protein Level and Axonal Transport of Mitochondria. PLoS Genet. 2012; 8:e1002537. [PubMed: 22396657]

Lutas A, Wahlmark CJ, Acharjee S, Kawasaki F. Genetic analysis in Drosophila reveals a role for the mitochondrial protein p32 in synaptic transmission. G3. 2012; 2:59–69. [PubMed: 22384382]

MacAskill AF, Atkin TA, Kittler JT. Mitochondrial trafficking and the provision of energy and calcium buffering at excitatory synapses. Eur J Neurosci. 2010; 32:231–240. [PubMed: 20946113]

Macaskill AF, Rinholm JE, Twelvetrees AE, Arancibia-Carcamo IL, Muir J, Fransson A, Aspenstrom P, Attwell D, Kittler JT. Miro1 is a calcium sensor for glutamate receptor-dependent localization of mitochondria at synapses. Neuron. 2009; 61:541–555. [PubMed: 19249275]

Malhotra JD, Kaufman RJ. ER stress and its functional link to mitochondria: role in cell survival and death. Cold Spring Harb Perspect Biol. 2011; 3:a004424. [PubMed: 21813400]

Manders EMM, Verbeek FJ, Aten JA. Measurement of Colocalization of Objects in Dual-Color Confocal Images. J Microsc. 1993; 169:375–382.

Mbefo MK, Paleologou KE, Boucharaba A, Oueslati A, Schell H, Fournier M, Olschewski D, Yin G, Zweckstetter M, Masliah E, et al. Phosphorylation of synucleins by members of the Polo-like kinase family. J Biol Chem. 2010; 285:2807–2822. [PubMed: 19889641]

McCormack JG, Halestrap AP, Denton RM. Role of calcium ions in regulation of mammalian intramitochondrial metabolism. Physiol Rev. 1990; 70:391–425. [PubMed: 2157230]

Messina A, Neri M, Perosa F, Caggese C, Marino M, Caizzi R, De Pinto V. Cloning and chromosomal localization of a cDNA encoding a mitochondrial porin from Drosophila melanogaster. FEBS Lett. 1996; 384:9–13. [PubMed: 8797793]

Mitra K, Rikhy R, Lilly M, Lippincott-Schwartz J. DRP1-dependent mitochondrial fission initiates follicle cell differentiation during Drosophila oogenesis. J Cell Biol. 2012; 197:487–497. [PubMed: 22584906]

Murley A, Lackner LL, Osman C, West M, Voeltz GK, Walter P, Nunnari J. ER-associated mitochondrial division links the distribution of mitochondria and mitochondrial DNA in yeast. eLife. 2013; 2:e00422. [PubMed: 23682313]

Nguyen TT, Oh SS, Weaver D, Lewandowska A, Maxfield D, Schuler MH, Smith NK, Macfarlane J, Saunders G, Palmer CA, et al. Loss of Miro1-directed mitochondrial movement results in a novel murine model for neuron disease. Proc Natl Acad Sci USA. 2014; 111:E3631–3640. [PubMed: 25136135]

Ouyang Y, Petritsch C, Wen H, Jan L, Jan YN, Lu B. Dronc caspase exerts a non-apoptotic function to restrain phospho-Numb-induced ectopic neuroblast formation in Drosophila. Development. 2011; 138:2185–2196. [PubMed: 21558368]

Perocchi F, Gohil VM, Girgis HS, Bao XR, McCombs JE, Palmer AE, Mootha VK. MICU1 encodes a mitochondrial EF hand protein required for Ca(2+) uptake. Nature. 2010; 467:291–296. [PubMed: 20693986]

Pilling AD, Horiuchi D, Lively CM, Saxton WM. Kinesin-1 and Dynein are the primary motors for fast transport of mitochondria in Drosophila motor axons. Mol Biol Cell. 2006; 17:2057–2068. [PubMed: 16467387]

Rizzuto R, Brini M, Murgia M, Pozzan T. Microdomains with high Ca2+ close to IP3-sensitive channels that are sensed by neighboring mitochondria. Science. 1993; 262:744–747. [PubMed: 8235595]

Rizzuto R, De Stefani D, Raffaello A, Mammucari C. Mitochondria as sensors and regulators of calcium signalling. Nat Rev Mol Cell Biol. 2012; 13:566–578. [PubMed: 22850819]

Rizzuto R, Pinton P, Carrington W, Fay FS, Fogarty KE, Lifshitz LM, Tuft RA, Pozzan T. Close contacts with the endoplasmic reticulum as determinants of mitochondrial Ca2+ responses. Science. 1998; 280:1763–1766. [PubMed: 9624056]

Rowland AA, Voeltz GK. Endoplasmic reticulum-mitochondria contacts: function of the junction. Nat Rev Mol Cell Biol. 2012; 13:607–625. [PubMed: 22992592]

Rozeboom AM, Pak DT. Identification and functional characterization of polo-like kinase 2 autoregulatory sites. Neurosci. 2012; 202:147–157.

Sanz A, Soikkeli M, Portero-Otin M, Wilson A, Kemppainen E, McIlroy G, Ellila S, Kemppainen KK, Tuomela T, Lakanmaa M, et al. Expression of the yeast NADH dehydrogenase Ndi1 in Drosophila confers increased lifespan independently of dietary restriction. Proc Natl Acad Sci USA. 2010; 107:9105–9110. [PubMed: 20435911]

Saotome M, Safiulina D, Szabadkai G, Das S, Fransson A, Aspenstrom P, Rizzuto R, Hajnoczky G. Bidirectional Ca2+-dependent control of mitochondrial dynamics by the Miro GTPase. Proc Natl Acad Sci USA. 2008; 105:20728–20733. [PubMed: 19098100]

Schon EA, Area-Gomez E. Mitochondria-associated ER membranes in Alzheimer disease. Mol Cell Neurosci. 2013; 55:26–36. [PubMed: 22922446]

Schon EA, Przedborski S. Mitochondria: the next (neurode)generation. Neuron. 2011; 70:1033–1053. [PubMed: 21689593]

Sheng ZH, Cai Q. Mitochondrial transport in neurons: impact on synaptic homeostasis and neurodegeneration. Nat Rev Neurosci. 2012; 13:77–93. [PubMed: 22218207]

Shim J, Mukherjee T, Mondal BC, Liu T, Young GC, Wijewarnasuriya DP, Banerjee U. Olfactory control of blood progenitor maintenance. Cell. 2013; 155:1141–1153. [PubMed: 24267893]

Song Y, Lu B. Regulation of cell growth by Notch signaling and its differential requirement in normal vs. tumor-forming stem cells in Drosophila. Genes Dev. 2011; 25:2644–2658. [PubMed: 22190460]

Stowers RS, Megeath LJ, Gorska-Andrzejak J, Meinertzhagen IA, Schwarz TL. Axonal transport of mitochondria to synapses depends on milton, a novel Drosophila protein. Neuron. 2002; 36:1063–1077. [PubMed: 12495622]

Tait SW, Green DR. Mitochondria and cell signalling. J Cell Sci. 2012; 125:807–815. [PubMed: 22448037]

Tang TS, Slow E, Lupu V, Stavrovskaya IG, Sugimori M, Llinas R, Kristal BS, Hayden MR, Bezprozvanny I. Disturbed Ca2+ signaling and apoptosis of medium spiny neurons in Huntington's disease. Proc Natl Acad Sci USA. 2005; 102:2602–2607. [PubMed: 15695335]

Teixeira FK, Sanchez CG, Hurd TR, Seifert JR, Czech B, Preall JB, Hannon GJ, Lehmann R. ATP synthase promotes germ cell differentiation independent of oxidative phosphorylation. Nat Cell Biol. 2015; 17:689–696. [PubMed: 25915123]

Terhzaz S, Southall TD, Lilley KS, Kean L, Allan AK, Davies SA, Dow JA. Differential gel electrophoresis and transgenic mitochondrial calcium reporters demonstrate spatiotemporal filtering in calcium control of mitochondria. J Biol Chem. 2006; 281:18849–18858. [PubMed: 16670086]

Tu H, Nelson O, Bezprozvanny A, Wang Z, Lee SF, Hao YH, Serneels L, De Strooper B, Yu G, Bezprozvanny I. Presenilins form ER Ca2+ leak channels, a function disrupted by familial Alzheimer's disease-linked mutations. Cell. 2006; 126:981–993. [PubMed: 16959576]

Venkatesh K, Hasan G. Disruption of the IP3 receptor gene of Drosophila affects larval metamorphosis and ecdysone release. Curr Biol. 1997; 7:500–509. [PubMed: 9273145]

Vos M, Lauwers E, Verstreken P. Synaptic mitochondria in synaptic transmission and organization of vesicle pools in health and disease. Front Synaptic Neurosci. 2010; 2:139. [PubMed: 21423525]

Wallace DC. A mitochondrial paradigm of metabolic and degenerative diseases, aging, and cancer: a dawn for evolutionary medicine. Annu Rev Genet. 2005; 39:359–407. [PubMed: 16285865]

Wallace DC. The epigenome and the mitochondrion: bioenergetics and the environment [corrected]. Genes Dev. 2010; 24:1571–1573. [PubMed: 20679390]

Wang H, Ouyang Y, Somers WG, Chia W, Lu B. Polo inhibits progenitor self-renewal and regulates Numb asymmetry by phosphorylating Pon. Nature. 2007; 449:96–100. [PubMed: 17805297]

Wang X, Schwarz TL. The mechanism of Ca2+ -dependent regulation of kinesin-mediated mitochondrial motility. Cell. 2009; 136:163–174. [PubMed: 19135897]

Wang X, Winter D, Ashrafi G, Schlehe J, Wong YL, Selkoe D, Rice S, Steen J, Lavoie MJ, Schwarz TL. PINK1 and Parkin Target Miro for Phosphorylation and Degradation to Arrest Mitochondrial Motility. Cell. 2011; 147:893–906. [PubMed: 22078885]

Wu Z, Sawada T, Shiba K, Liu S, Kanao T, Takahashi R, Hattori N, Imai Y, Lu B. Tricornered/NDR kinase signaling mediates PINK1-directed mitochondrial quality control and tissue maintenance. Genes Dev. 2013; 27:157–162. [PubMed: 23348839]

Highlights

- Mitochondrial Rho GTPase Miro regulates NSC maintenance and lineage maturation
- Miro controls mitochondrial Ca^{2+} homeostasis independent of its role in transport
- Miro interacts with Ca^{2+} transporters at the ER-mitochondria contact site (ERMCS)
- Miro activity is positively regulated by Polo kinase through phosphorylation

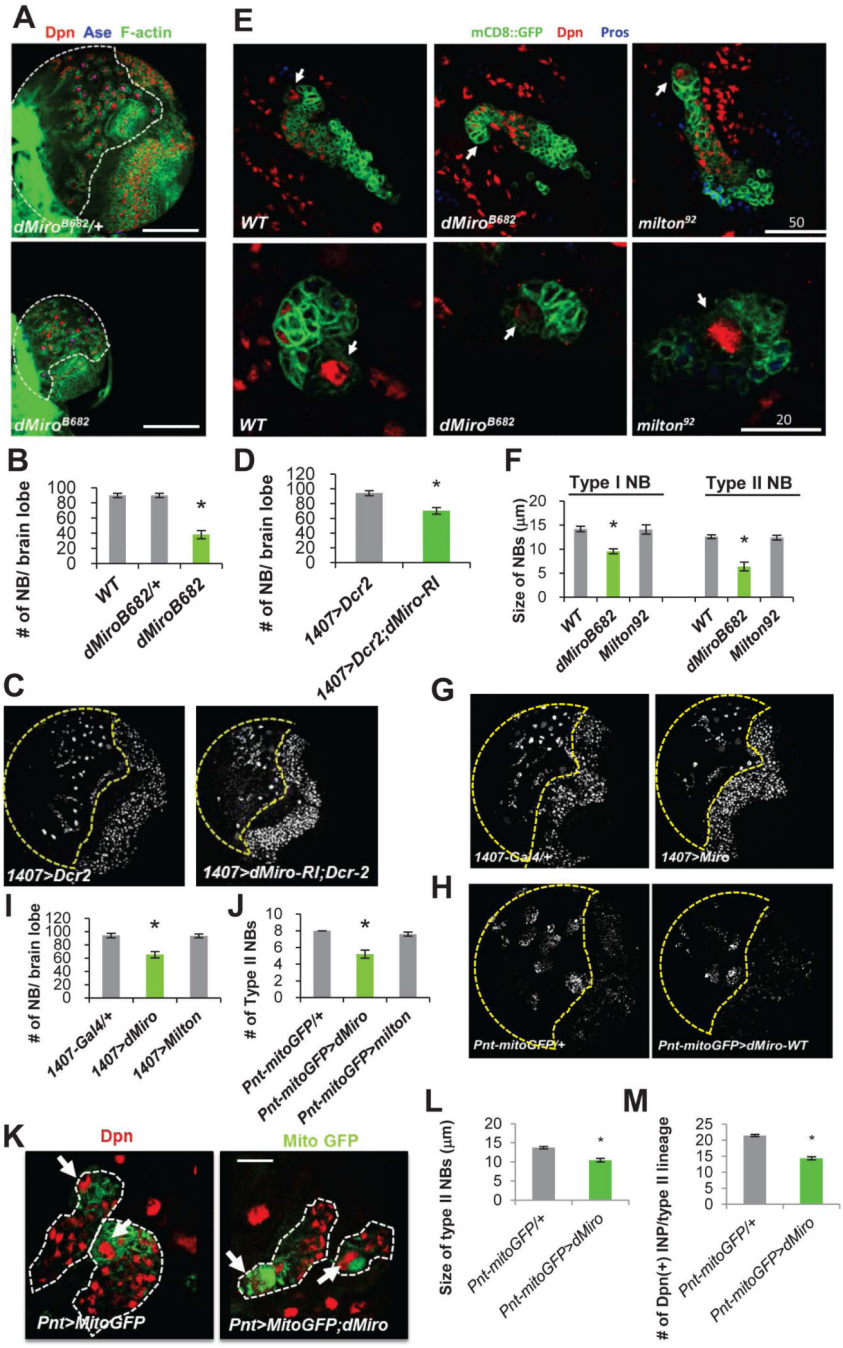

Figure 1. Regulation of NB Behavior by Miro

(A, B) Reduction of NB number and brain size in *dMiro*^{B682} null mutant. Larval brains of *dMiro*^{B682} heterozygous and homozygous animals were immunostained for pan-NB marker Dpn, type I NB marker Ase, and actin. The central brain area is outlined with white dashed line.

(C, D) Reduction of NB number by NB-specific knockdown of dMiro. Control (*1407>Dcr2*) and dMiro RNAi (*1407>Dcr2,dMiro-RI*) larval brains were immunostained for Dpn.

(E) MARCM analysis of NB lineages in the *dMiro*^{B682} and *milton*^{92} backgrounds. Brains were stained for Dpn and Pros, a differentiation marker. NB clones are marked with GFP. Upper: Type II NBs, Lower: Type I NBs. Primary NBs are indicated with arrows. Note that the primary NB in the *dMiro*^{B682} type II NB clone is losing Dpn expression.

(F) Quantification of the size of NBs from E.

(G, H) Effects on NB number by pan-NB (*1407-Gal4*) or type II NB-specific (*Pnt-Gal4*) dMiro OE. Brains were stained for Dpn. The central brain area is outlined with yellow dashed line.

(I, J) Quantification of total NB (I) or type II NB (J) number from G and H, respectively.

(K-M) Effects of dMiro OE on type II NB size (L) and IP number (M). The type II NB lineages are outlined with white dashed line. Primary NBs are marked with arrows.

Error bar: SEM; *, $p<0.05$ versus control in Student's *t*-tests. n = 5. Scale bars, 100 μm (A, C, G); 20 μm (K).

See also Figure S1.

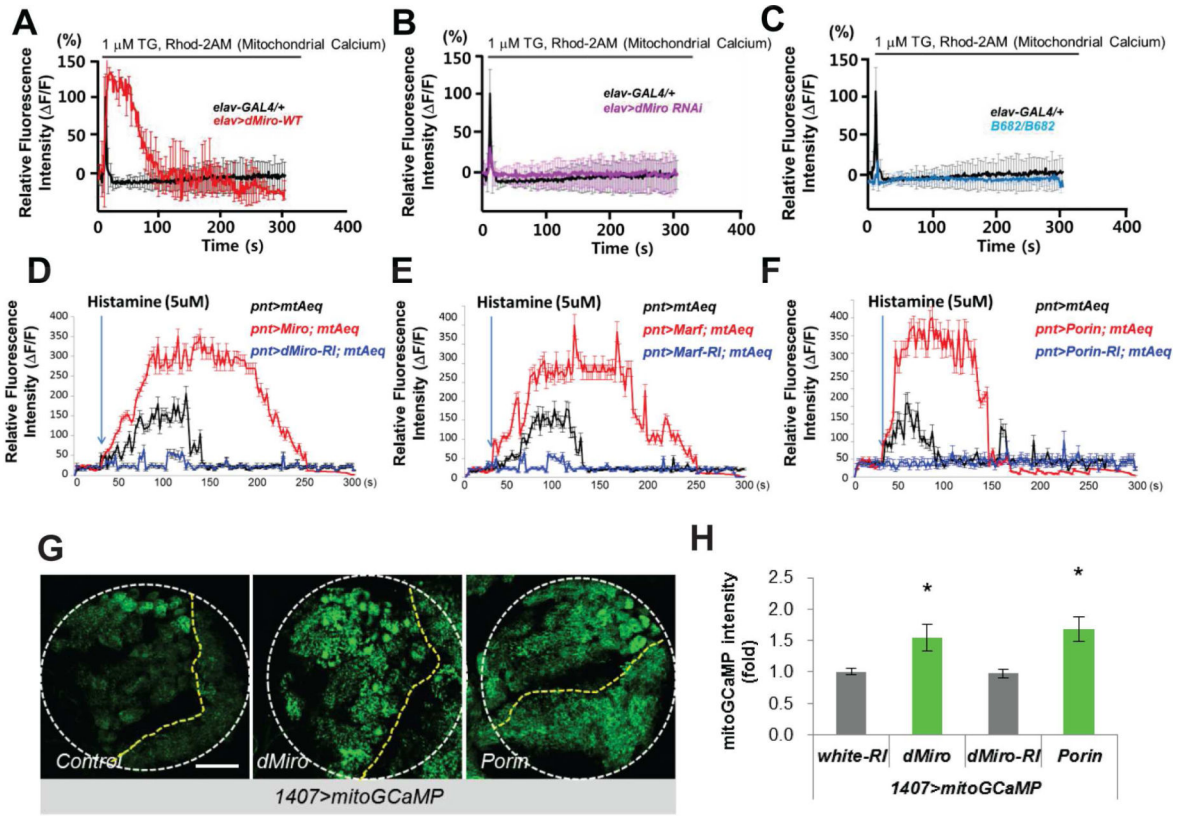

Figure 2. Regulation of Ca^{2+}_{mito} by Miro

(A-C) Effects of pan-neuronal *elav-Gal4* driven dMiro OE (A) or dMiro RNAi (B), or $dMiro^{B682}$ null mutation (C), on TG-stimulated Rhod-2 AM fluorescence in primary cultured fly neurons. The traces show mean response of cells present in the microscope field and are representative of more than 3 experiments.

(D-F) Effects of OE or RNAi of Miro (D), Marf (E), or Porin (F) on mitochondrial Ca^{2+} in type II NB lineages as monitored using mito-AEQ. The traces show mean response of 10 dissected larval brains present in the microtiter plate and are representative of more than 3 tests.

(G, H) Imaging of basal Ca^{2+}_{mito} using mito-GCaMP in larval brains without (control) or with Miro or Porin OE. White circle outline larval brain, yellow lines separate central brain (left) from the rest of brain. Images are representative of more than 5 samples. H, quantification of mito-GCaMP intensity in NBs from G.

Error bar: SEM; *, $p<0.05$ versus control in Student's *t*-tests. Scale bars, 100 μm (G).

See also Figure S2.

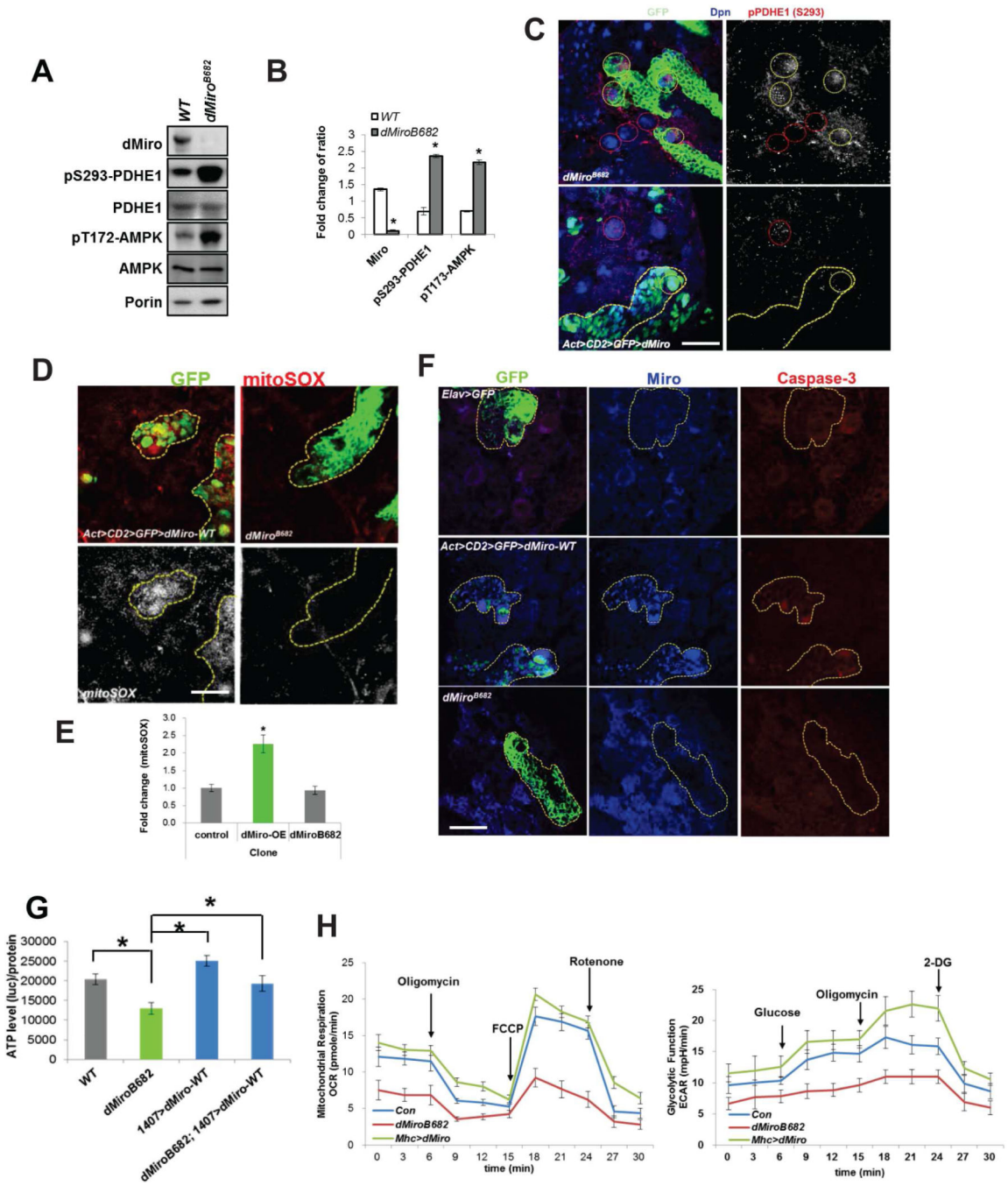

Figure 3. Miro-Mediated Ca^{2+}_{mito} Homeostasis Regulates Mitochondrial Activity

(A, B) Western blot (WB) analysis showing increased p-PDHE1 and p-AMPK in *dMiro* mutant. PDHE1, Porin, and actin serve as controls. Normalized protein levels are shown as the ratio of dMiro/Porin, pS293-PDHE1/PDHE1 and pT713-AMPK/AMPK from A. (C-F) Immunostaining of p-PDHE1 (C), mito-SOX (D, E), or activated caspase 3 (F) in *dMiro* mutant MARCM clones (yellow-outlined in upper panels) or dMiro-OE Flip-out clones (yellow-outlined in lower panels). NBs within clones are marked with white circles and control NBs outside of the clones are marked with red circles in C.

(G) Effect of dMiro-WT OE on ATP level in *dMiro* mutant larval brain.
(H) Real-time changes in OCR and Glycolytic rate (ECAR) were measured in control, dMiro-WT-OE (*Mhc>dMiro-WT*) and *dMiro* mutant animals using the Seahorse Bioscience XF Analyzer.
Error bar: SEM; *, $p<0.05$ versus control in Student's *t*-tests. Scale bars, 50 μm (C), 20 μm (D, E).
See also Figure S3.

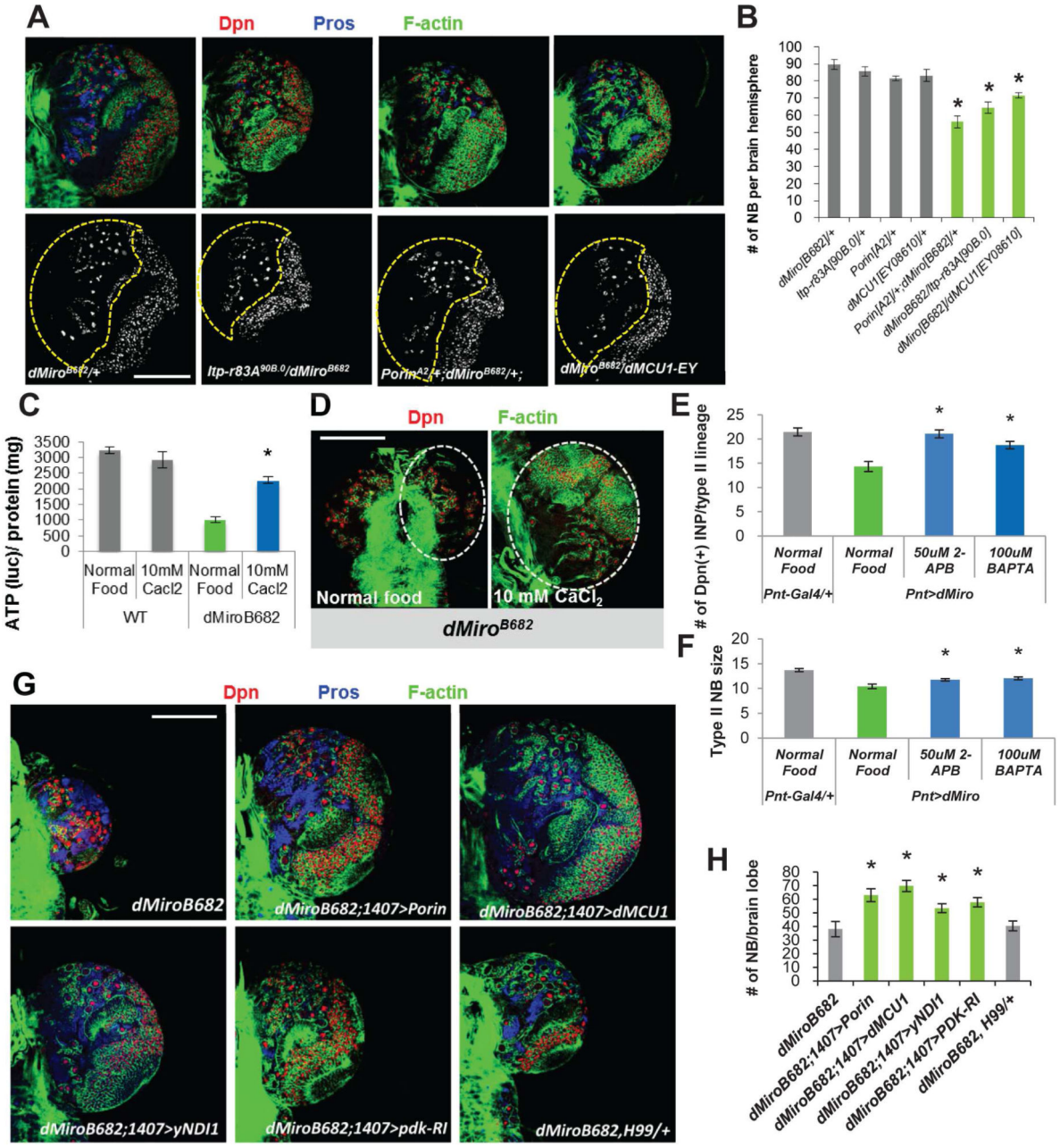

Figure 4. Functional Interaction between Miro and Ca^{2+} Transporter at the ERMCS

(A, B) Transheterozygotes between *dMiro* and *IP3R (Itp-r83A)*, *Porin*, or *dMCU* mutants resulted in reduction of NB number. Larval brains were immunostained for Dpn, Pros, and F-actin (cell cortex). Central brain area is outlined with dashed line.

(C, D) Effects of $CaCl_2$ feeding in rescuing brain ATP level (C) and brain size (D) of *dMiro* mutant. Larval brains were immunostained for Dpn and F-actin. Brain lobes are outlined.

(E, F) Quantification of the effects of 2-APB and BAPTA feeding in rescuing the reduced IP number (E) and NB size (F) caused by dMiro OE.

(G, H) Genetic interactions showing rescue of NB number in *dMiro* mutant by the OE of Porin, dMCU, yNDI1, or PDK-RNAi, but not the *H99* heterozygous background. Larval

brains were immunostained for Dpn, Pros, and F-actin. H, quantification of number of NBs shown in G.

Error bar: SEM; *, $p<0.05$ in Student's *t*-tests. Scale bars, 100 μm.

See also Figure S4.

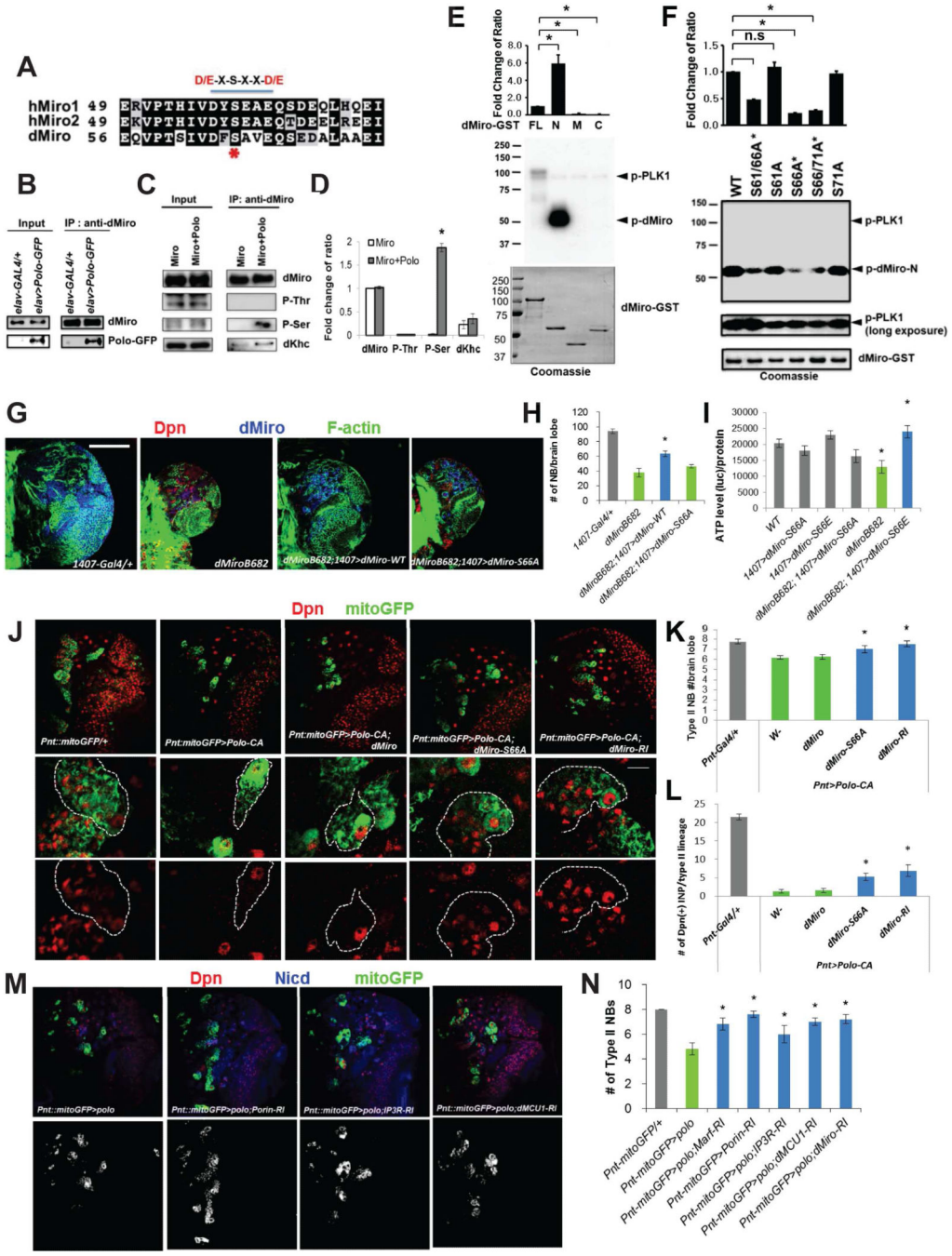

Figure 5. Regulation of Miro Function by Polo-Mediated Phosphorylation at Serine 66

(A) Comparison of candidate Polo/PLK phosphorylation motifs at the N-terminus of Miro. The consensus D/E-X-S-X-X-D/E motif is underlined, and S66 indicated by asterisk.

(B) Polo-GFP is present in dMiro IP prepared from fly brain extracts.

(C, D) Increased dMiro phosphorylation at Ser but not Thr residue(s) after Polo co-expression in fly brain. D, quantification of normalized phospho-Ser intensity from C.

(E, F) *In vitro* kinase assays showing phosphorylation of dMiro-N by PLK1 (E), and the strong effect of S66A mutation in blocking PLK1 effect (F). Bar graph shows quantification

of normalized phospho-dMiro signal (top). GST-dMiro proteins were visualized by autoradiography (middle panels) or Coomassie blue staining (bottom panels).
(G, H) Rescue of brain size (G) and NB number (H) in *dMiro* mutant by dMiro-WT but not -S66A. Larval brains were immunostained for Dpn, Pros, and F-actin.
(I) Rescue of reduced brain ATP level in *dMiro* mutant by dMiro-S66E, but not -S66A.
(J-L) Rescue of type II NB number (J, K) or IP number (J, L) in Polo-CA OE animals by dMiro-S66A or dMiro-RNAi. Larval brains were immunostained for Dpn and GFP. Dashed lines mark type II NB lineages.
(M, N) Rescue of type II NB number in Polo OE animals by RNAi of ERMCS components. Larval brains were immunostained for Dpn, GFP and NICD (cell membrane). N, quantification of number of NBs in M.
Error bar: SEM; *, $p<0.05$ in Student's *t*-tests. Scale bars, 100 μm (G, upper panel of J, M), 20 μm (lower panel of J).
See also Figure S5.

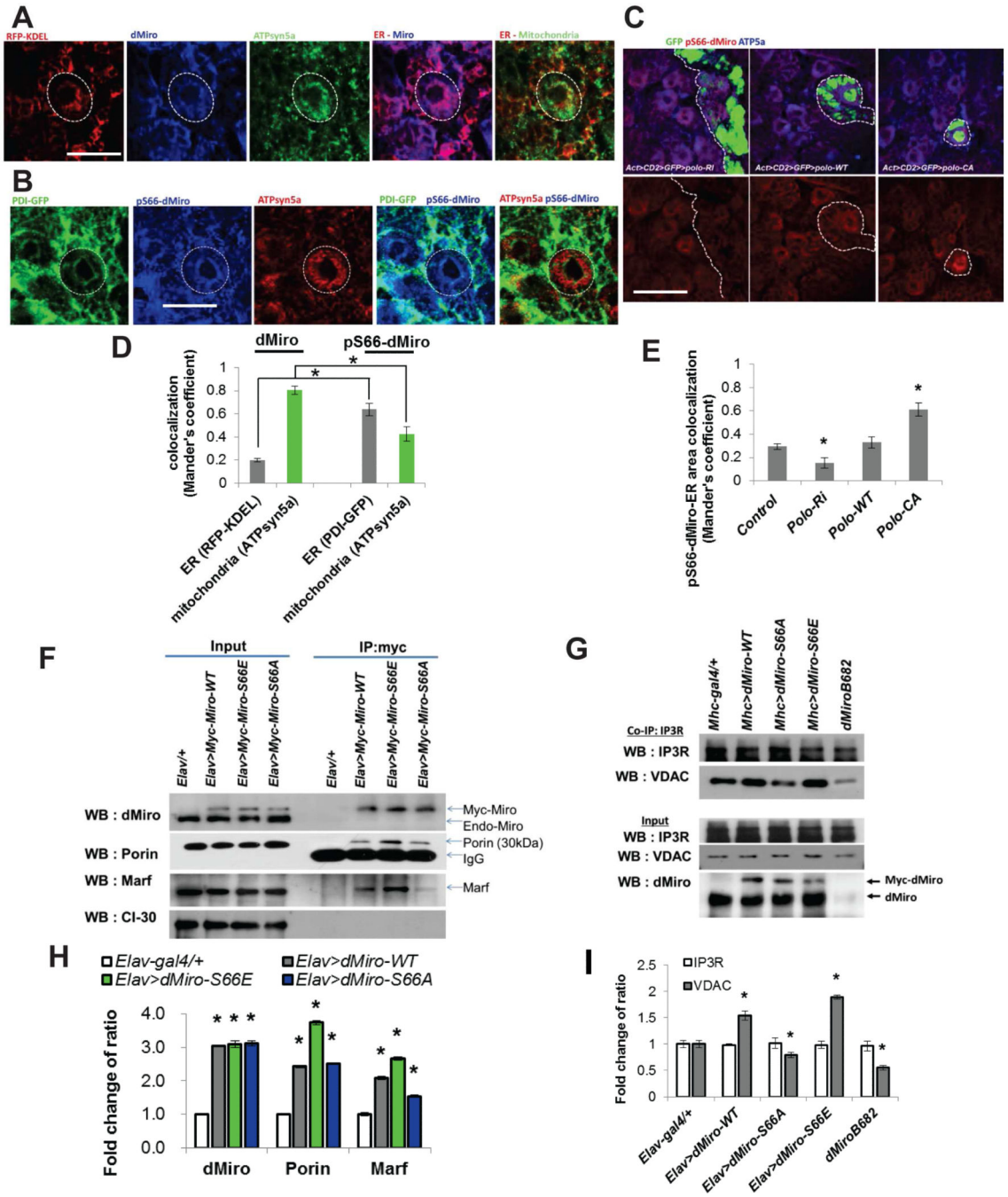

Figure 6. Phosphorylation of Miro Regulates the Integrity of ERMCS

(A, B) Immunostaining showing localization of p-S66-Miro to ERMCS of larval brain NBs. Circles mark the NBs of interest. Larval brains were stained for the indicated antibodies.

(C) Effects of Polo on p-S66-Miro immunosignal in Flip-out NB clones with Polo overexpressed or knocked down by RNAi. Clones are marked with GFP.

(D, E) Quantification of dMiro and p-dMiro colocalization with ER and mitochondria shown in A and B (D) or p-dMiro colocalization with ER shown in C (E), using Mander's coefficient.

(F, H) Co-IP assays showing the effects of S66A and S66E mutations on Miro interaction with Porin and Marf. H, quantification of proteins pulled down by co-IP in F.
(G, I) Co-IP assays showing the effects of *dMiro* mutation or OE of Miro variants on IP3R-VDAC interaction. I, quantification of proteins pulled down by co-IP in G.
Error bar: SEM; *, $p<0.05$ in Student's *t*-tests. Scale bars, 20 μm.
See also Figure S6.

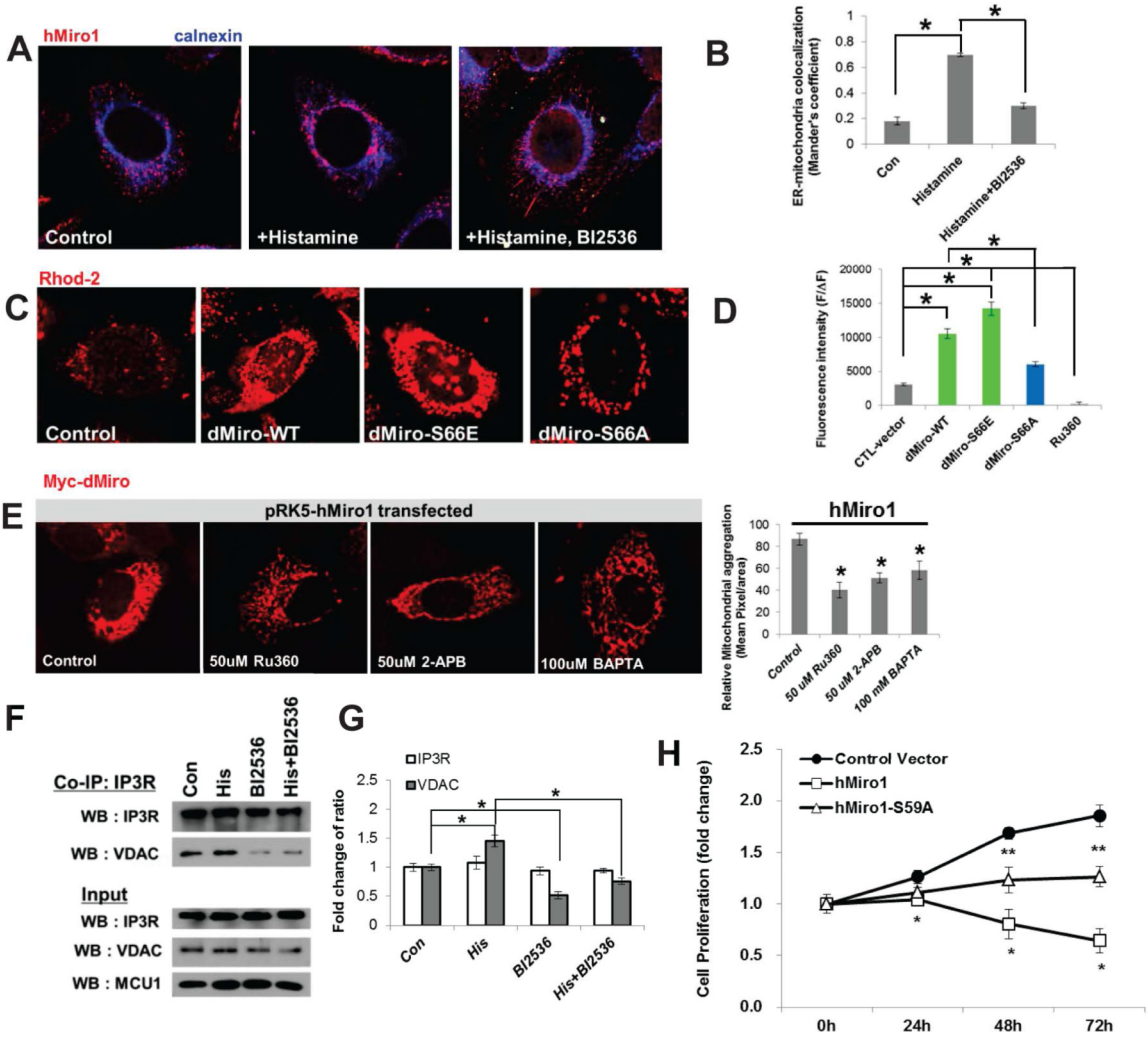

Figure 7. Regulation of Ca^{2+}_{mito} by Miro in Mammalian Cells

(A, B) Immunostaining showing that the PLK inhibitor BI2536 blocked histamine-induced hMiro1 recruitment to perinuclear ER area in HeLa cells. B, quantification of Miro-Calnexin colocalization using Mander's coefficient.

(C, D) Effects of dMiro variants on Rhod-2 AM fluorescence in HeLa cells. D, quantification of Rhod-2 signals. RU360 treatment serves as control.

(E) Effects of pharmacological intervention of ER-mitochondrial Ca^{2+} transfer (RU360, 2-APB) or Ca^{2+} availability (BAPTA) on hMiro1-induced mitochondrial morphology change visualized with mitochondria-localized hMiro. Bar graph shows quantification of mitochondrial aggregation.

(F, G) Co-IP assay showing effect of PLK inhibition on IP3R-VDAC interaction in HeLa cells. G, quantification of signal intensity change shown in F.

(H) Effects of hMiro1-WT and hMiro1-S59A transfection on mammalian NSC (ReNcell CX) proliferation monitored over a 72h time course.

Error bar: SEM; *, $p<0.05$ in Student's t-tests. Scale bars, 100 μm.

See also Figure S7.